On the modelling of microsegregation in steels involving thermodynamic databases

IOP Conf. Series: Materials Science and Engineering **119** (2016) 012027 doi:10.1088/1757-899X/119/1/012027

On the modelling of microsegregation in steels involving thermodynamic databases

D You, C Bernhard, S Michelic, G Wieser and P Presoly

Chair of Ferrous Metallurgy, Montanuniversität Leoben, Franz-Josef-Straße 18, 8700 Leoben, Austria

E-mail: dali.you@stud.unileoben.ac.at

Abstract. A microsegregation model involving thermodynamic database based on Ohnaka's model is proposed. In the model, the thermodynamic database is applied for equilibrium calculation. Multicomponent alloy effects on partition coefficients and equilibrium temperatures are accounted for. Microsegregation and partition coefficients calculated using different databases exhibit significant differences. The segregated concentrations predicted using the optimized database are in good agreement with the measured inter-dendritic concentrations.

1. Introduction

Microsegregation results from solute partitioning at the dendritic scale during solidification. This phenomenon can lead to the formation of defects during the casting process (e.g., hot tearing) and also negatively affect the product quality (inhomogeneous microstructure and undesirable primary precipitates). Hence, it is not surprising that this research topic has already been intensively investigated by several research groups in the past[1-6].

Existing modeling approaches consist of numerical and analytical models. Numerical solutions, depending on the magnitude of model building, are typically complex to solve. Process models are constrained by the need to save calculation time. Therefore, these models generally refer to simple analytical approaches. More elaborate software products are DICTRA®[7] and IDS®[8], which are widely applied for solving diffusion and phase transformation problems[9-11]. The present concept applies an easily solvable analytical model coupled with the thermodynamic library ChemApp®[12] and with both commercial and self-optimized databases in the background. The optimization of the databases is an ongoing activity and based on extensive DSC measurements of high-temperature phase transformations in Fe-C-Si-Mn-Al systems[13]. More details are described in the paper "*Thermodynamic optimization of individual steel databases by means of systematic DSC measurement*" which is also submitted to this conference. In future research, the proposed model will be coupled with a phase nucleation model to take the formation of non-metallic inclusions above the liquidus and during solidification into account.

2. Model description

In the proposed model, microsegregation was calculated using Ohnaka's model. Thermodynamic equilibrium calculation was performed using ChemApp and selected thermodynamic databases. ChemApp is an interface software developed by GTT Technologies, Herzogenrath, Germany. It may be linked with a source code written in FORTRAN, C/C++, Visual Basic® and Borland Delphi®. In this case, FORTRAN was applied as the programming language. Microsoft Visual Studio 2013 was used as a main frame provider and modern compiler. The schematic of the model is described by Figure 1.

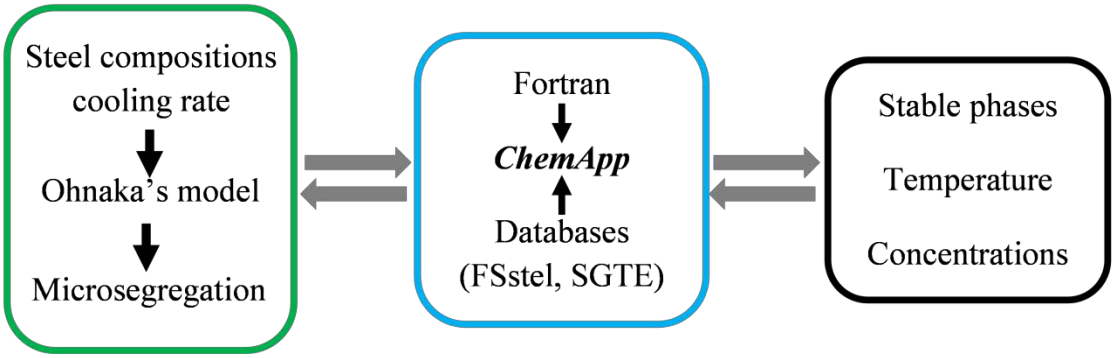

Figure 1. Schematic of the microsegregation model.

2.1. Analytical equation

For considering the changes of the partition and diffusion coefficients, Ohnaka's model was integrated into Equation 1. Local partition coefficients and diffusion coefficients were calculated at each solidification step, but within the increase of solid fraction by Δf_s, they were assumed to be constants.

$$C_L^+ = C_L\{\frac{1-\Gamma\cdot f_s}{1-\Gamma\cdot(f_s+\Delta f_s)}\}^{\frac{1-k}{\Gamma}}, \text{ with } \Gamma = 1-\frac{4\alpha k}{1+4\alpha} \quad (1)$$

$$\alpha = \frac{4D_s t_f}{(\lambda_2)^2} \quad (2)$$

where f_s represents the solid fraction; C_L^+ and C_L are the concentrations of solutes in the residual liquid at solid fractions of f_s and $f_s + \Delta f_s$, respectively; k is the equilibrium partition coefficient between solid and liquid; α is the back diffusion coefficient, which can be calculated using Equation 2; D_s is the solute diffusion coefficient in solid; t_f is the local solidification time; and λ_2 is the secondary dendrite arm spacing.

2.2. Parameters

In the applied model, temperatures at the solidification interface and partition coefficients (k) were calculated using ChemApp. At each solidification step, for a multicomponent system, the phase transformation point from liquid to solid was detected after the activity of δ-ferrite or austenite approached one. Then, the concentrations of solutes in both liquid and solid and the temperature were determined. For simplification, Figure 2 describes a binary system of the above process. The diffusion coefficients (D_S) applied in the calculations are listed in Table 1.

The partition and diffusion coefficients used for the calculations were the average of the values between the current and former steps. The temperatures were updated in a loop until the difference between two adjacent values was less than 10^{-3} K.

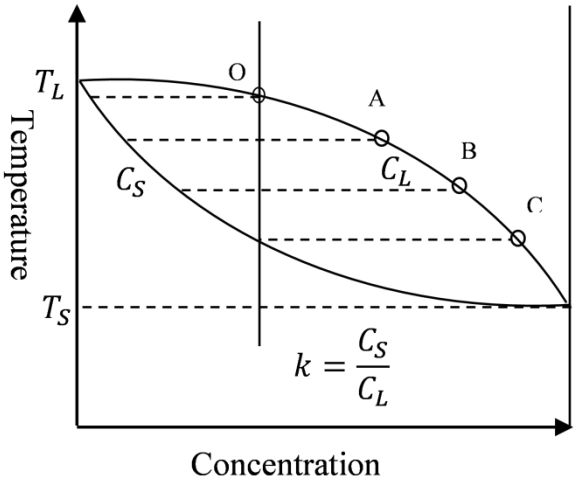

Figure 2. Schematic illustration of the determination of partition coefficients and temperatures.

Table 1. Diffusion coefficients of solutes.[14-16]

Elements	D_δ [a] (m^2s^{-1})	D_γ [a] (m^2s^{-1})
C	0.0127Exp(-81301/RT)	0.0761Exp(-134429/RT)
Si	8.0Exp(-248710/RT)	0.3Exp(-251218/RT)
Mn	0.76Exp(-116935/RT)	0.055Exp(-249128/RT)
P	2.9Exp(-229900/RT)	0.01Exp(-182666/RT)
S	4.56Exp(-214434/RT)	2.4Exp(-212232/RT)
Al	5.9Exp(-241186/RT)	5.15Exp(-245800/RT)

[a] R: 8.314 J/(K·mol); T: temperature in Kelvin.

Secondary dendrite arm spacing was estimated using Equation 3, which is influenced by the local solidification time and initial carbon content.[17] In the first step, the local solidification time is estimated. In the second step, the local solidification time is calculated according to Equation 4 after obtaining the solidus temperature. This process was repeated until the difference between two adjacent local solidification times was less than 10^{-4} seconds,

$$\lambda_2 = (27.3 - 13.1C_0^{\frac{1}{3}})t_f^{\frac{1}{3}} \quad (3)$$

$$t_f = \frac{T_L - T_S}{R_c} \quad (4)$$

where λ_2 (μm) is the secondary dendrite arm spacing, C_0 is the initial concentration of carbon in mass percent, t_f (s) is the local solidification time, R_c (K/s) is the cooling rate, and T_L and T_S (K) are the liquidus and solidus temperatures, respectively.

In addition, the peritectic reaction was realized in a simple way similar to other analytical models. If ChemApp detects that the solid phase at the solidification interface will change from δ-ferrite to austenite, the partition and diffusion coefficients of austenite were applied.

3. Comparisons with characteristic temperatures

Zero strength temperature (ZST) is the critical temperature below which solidifying materials start to transmit strength inside the dendritic structure of both solid and liquid. Zero ductility temperature (ZDT) is defined as the temperature at which ductility first starts to increase during the solidification process. The schematic of ZST and ZDT is shown in Figure 3. Note that ZDT also stands for the non-equilibrium solidus temperature. Both ZST and ZDT are strongly influenced by solute enrichments and can comprehensively reflect the phenomenon. Additionally, hot tears generally form between ZST and ZDT; thus, it is also desirable to reasonably estimate ZST and ZDT through solidification modeling.

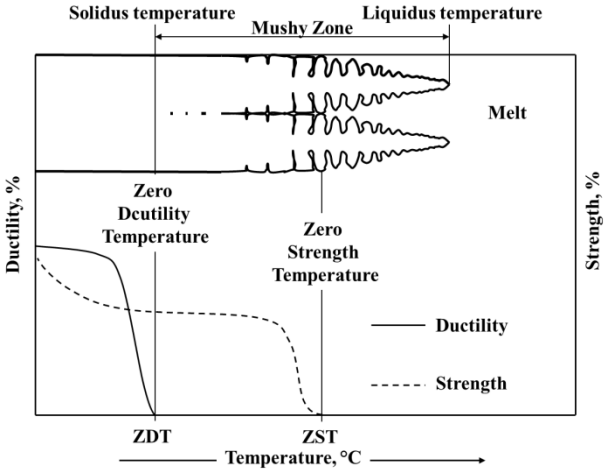

Figure 3. Schematic of ZST and ZDT. [18]

According to the statistical analysis and experimental results from Won[19], the temperatures at solid fractions of 0.75 and 0.99 were considered as ZST and ZDT. Note that the experimentally determined ZST values correspond with the calculated solid fractions of between 0.65 and 0.8, whereas ZDT commonly varies just between 0.98 and 1.0. Therefore, it cannot be expected that the ZST fits perfectly to the calculated solidus temperature for a solid fraction of 0.75.

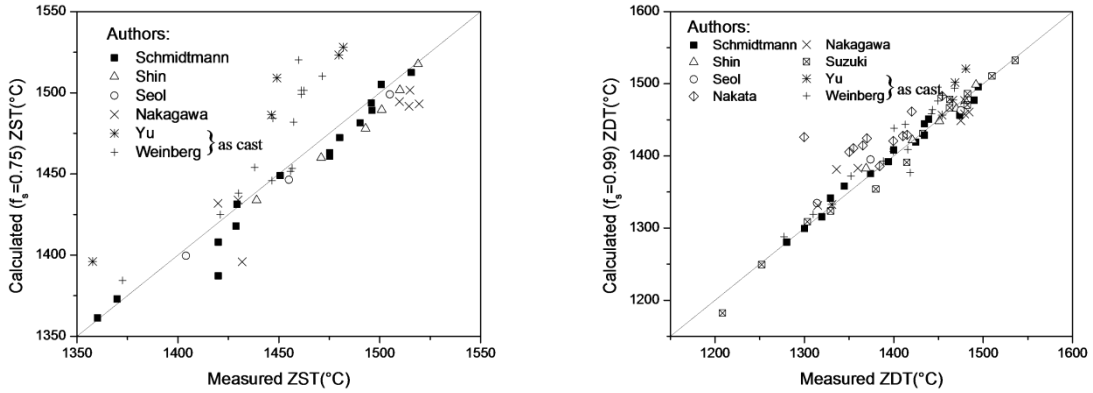

(a) (b)

Figure 4. Comparisons of (a) ZST and (b) ZDT between predicted and measured data.[20-27]

Figure 4 compares the ZST and ZDT from the calculated and measured data by different authors[20-27] for a certain range of steels. In this part, the calculations were carried out using FSstel database. Under the same given conditions of steel compositions and cooling rates, the calculated ZST and ZDT are in reasonable agreement with the experimental results. Note that the correspondence between the ZST from analysis and measured data is of rather poor quality. The main reason is that the ZST does not necessarily coincide with a solid fraction of 0.75 but rather depends on the steel composition; Shin et al.[21] found that the ZST varies between 0.6 and 0.7. In contrast, the correspondence of the calculated and measured ZDT is excellent. The above results, to some extent, illustrate the reasonability of the calculations. However, the comparisons of ZST and ZDT are only an inaccurate way to verify the microsegregation predictions.

4. Influence of different databases

In this section, three different databases, FSstel(FactSage 6.4[28]), SGTE2014 and an optimized SGTE version were applied to predict segregated concentrations of a TRIP steel. Among them, FSstel and SGTE2014 are commercial databases; the optimized SGTE is a 'private' one. An important information at this point is, that the Fe-C-Mn system is identical in all three databases and was not optimized. However, in the private database the manganese interaction with Si and Al were selectively optimized, based on model alloys and DSC measurements. The chemical composition of the selected steel is listed in Table 2. For comparing with the following measured results, secondary dendrite arm spacing was set to 18 μm and the local solidification time was calculated using Equation 3.

Table 2. Chemical compositions (mass%).

C	Si	Mn	Al
0.21	0.54	2.12	0.77

Figure 5 compares the results calculated with different databases. It shows that both solute concentrations and partition coefficients exhibit significant differences. The carbon concentration profiles (Figure 5 (a)) are similar until a solid fraction of 0.7 is reached, and then they differ; concentrations of silicon and manganese (Figure 5 (b) and Figure 5 (c)) predicted with FSstel database are close to those predicted with SGTE2014 database, while they are higher than those calculated by the private database; for aluminium, all the three calculations show its negative segregation, and the concentration in the residual liquid estimated with the private database is higher than those estimated with the other two databases.

The differences in the concentration profiles can be well explained by the differences in the corresponding partition coefficients. For positive segregation (carbon, silicon and manganese), the smaller partition coefficients indicate the higher segregation; while for negative segregation, the smaller partition coefficients lead to a lower segregation. Taking manganese as an example (Figure 5 (c)), the partition coefficient calculated using the private database is always larger than those calculated using the FSstel and SGTE2014 databases, which results in a lower concentration profile calculated with the private database. Note that the sharp changes of partition coefficients in Figure 5 are caused by the peritectic reaction. It shows that peritectic reaction times of different calculations vary with each other. At the same time, peritectic reaction leads to the decreases of back diffusions, which further increases the concentrations in residual liquid. This explains the higher concentrations calculated with the FSstel database for silicon and manganese between solid fraction 0.63 and 0.79, though their partition coefficients are larger (Figure 5 (b) and (c)). Different databases have their own parameters for the Gibbs energy minimization and thermodynamic equilibrium calculations.

Therefore, the partition coefficients and equilibrium concentrations calculated with different databases vary with each other.

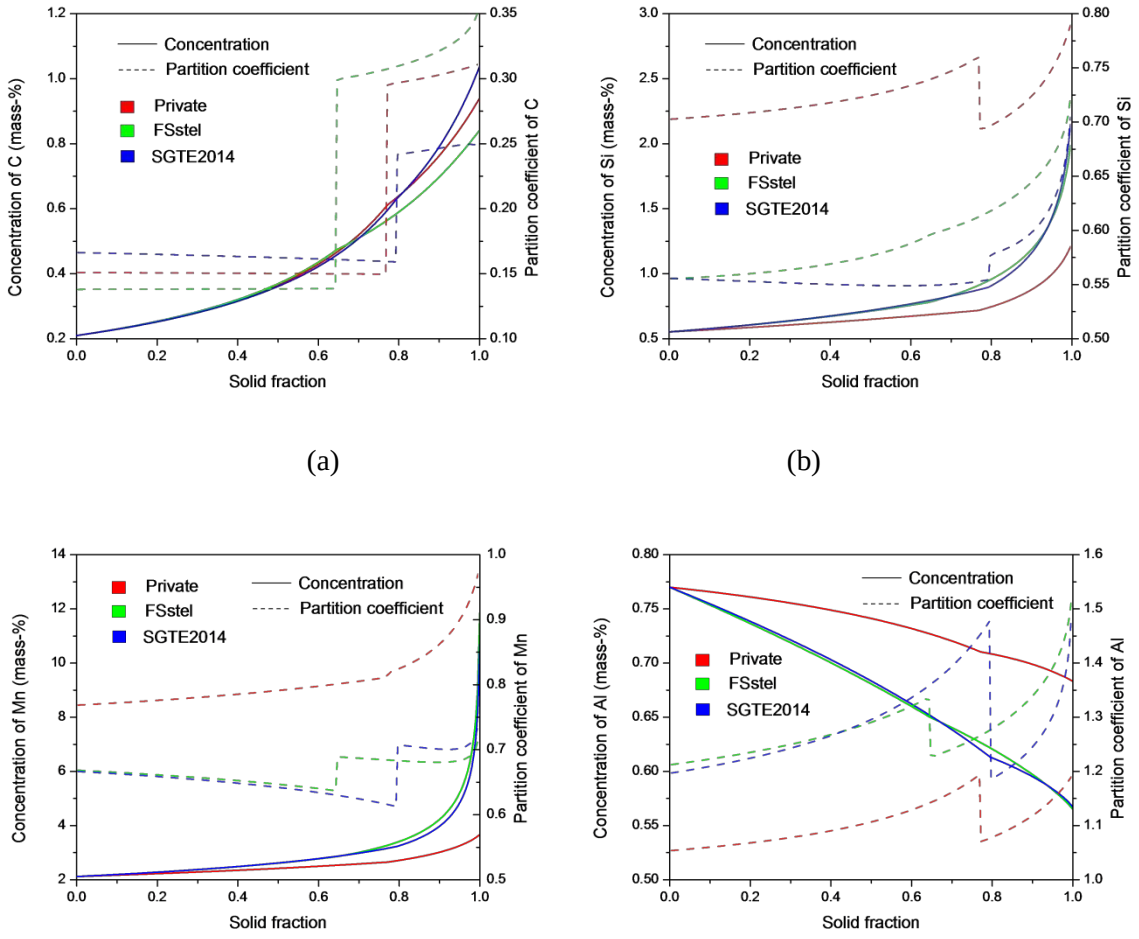

Figure 5. Predictions of segregated concentrations and partition coefficients with different databases (a) carbon, (b) silicon, (c) manganese and (d) aluminium.

For comparing with the predictions, a sample with the same compositions as listed in Table 2 was produced by means of high-frequency remelting and spin-casting. The small sample (60g) was solidified with high speed and water-quenched so that the back diffusions of solutes were minimized. Then, the microprobe analysis was performed on a selected cross section. The concentration distributions of the solutes are shown in Figure 6.

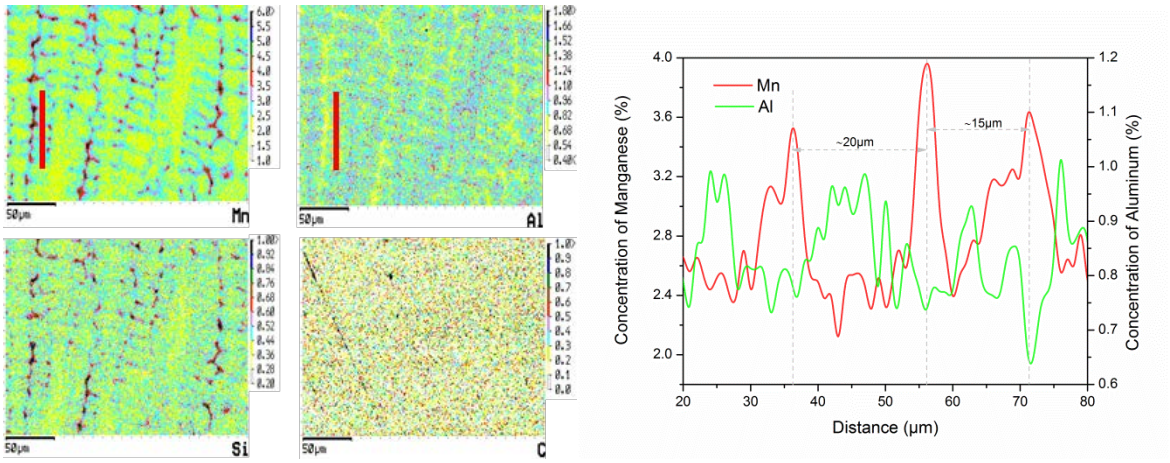

(a) (b)

Figure 6. Concentration distributions of (a) cross section and (b) line scan of secondary dendrites.

From Figure 6 (a), both primary and secondary structures are clearly drawn by the segregated concentrations of manganese, aluminium and silicon. The carbon concentration distributes quite evenly due to its fast diffusion. To evaluate the calculations, the concentration profile between two secondary dendrite arms was investigated in detail. A line scan was performed on the secondary dendrites as indicated by the red line in Figure 6 (a).

Figure 6 (b) describes the concentration distributions of manganese and aluminium over the line scan distance. Concentrations of manganese and aluminium reflect the microsegregation. Manganese gets enriched in inter-dendrite zones and approaches to the highest concentrations. By contrast, aluminium shows a negative segregation and reaches the lowest concentrations in inter-dendrite zones. Compared with the measurements, the segregated trends are predicted well by the proposed model. For the values, the measured inter-dendritic concentrations of manganese range from 3.4% to 4.0%. As shown in Figure 5 (c), the segregated concentration of manganese calculated with the private database is about 3.5% which fits well with the measured results. While for the predictions with the FSstel database and the SGTE2014 database, the final segregated concentrations exceed 10% which seems to be unrealistic. For aluminium, the measured inter-dendritic concentrations vary from 0.65% to 0.75%. The inter-dendritic concentration predicted with the private database of 0.68% is closer to the measured value than the results calculated with the other two databases (0.57%).

Based on the above discussion, the proposed model can better predict the microsegregation of the investigated TRIP steel with the private database. Optimization of the database is necessary to better describe the thermodynamic equilibrium of selected steels and the work is still ongoing in the current research group.

5. Summary

In the present study, Ohnaka's model was coupled with thermodynamic databases for predicting microsegregation of steels. The solute enrichment of a TRIP steel was calculated with two commercial and one private optimized thermodynamic databases. The results were compared with measured inter-dendritic concentrations of the selected experiment. According to the investigations, the following conclusions can be drawn:

- By coupling with a thermodynamic database, the present model offers new development space for simple analytical models.
- Using the private optimized database, solute enrichment of selected steels can be better predicted with the present model.
- The model can also function as a tool for giving feedback for the database optimization.

In future studies, using this model, the consideration of the precipitation of even very complex non-metallic phases (oxides and carbides) during solidification would be possible. Furthermore the coupling of the analytical microsegregation model with nucleation and growth kinetics for inclusions in steel is intended, opening many new areas of application.

Acknowledgements

The authors are grateful for the financial support from the Federal Ministry for Transport, Innovation and Technology (bmvit) and from the Austrian Science Fund (FWF): [TRP 266-N19].

References

[1] Scheil E 1942 *Z. Metallkd.* **34** 70
[2] Gulliver G H 1913 *J. Inst. Met.* **9** 120
[3] Brody H D and Flemings M C 1966 *Trans. TMS-AIME* **236** 615
[4] Clyne T W and Kurz W 1981 *Metall. Trans. A* **12A** 965
[5] Kobayashi S 1988 *J. Cryst. Growth* **88** 87
[6] Ohnaka I 1986 *Trans. Iron Steel Ins. Jpn.* **26** 1045
[7] Andersson O J, Helander T, Höglund L, Shi P and Sundman B 2002 *CALPHAD* **26** 273
[8] Miettinen J, Louhenkilpi S, Kytönen H and Laine J 2010 *Math. Comp. Sim.* **80** 1536
[9] Griesser S, Reid M, Pierer R, Bernhard C and Dippenaar R 2014 *Steel Res. Int.* **85** 1257
[10] Rudnizki J, Zeislmair B, Prahl U and Bleck W 2010 *Steel Res. Int.* **81** 472
[11] Röttger A, Weber S, Theisen W, Rajasekeran B and Vaßen R 2011 *Steel Res. Int.* **82** 671
[12] Petersen S, Hack K, Monheim P and Pickartz U 2007 *Int. J. Mater. Res.* **98** 946
[13] Presoly P, Pierer R and Bernhard C 2013 *Metall. Mater. Trans. A.* **44** 5377
[14] Yamada W, Matsumiya T and Ito A 1990 *Proc. 6th Int. Iron Steel Cong.* **1** 618.
[15] Ueshima Y, Mizoguchi S, Matsumiya T and Kajioka H 1986 *Metall. Trans. B* **17B** 845
[16] Bester H, Lange K W 1972 *Arch. Eisenhuttenwesen* **43** 207
[17] Pierer R and Bernhard C 2008 *J. Mater. Sci*. **43** 6938
[18] Won Y M, Yeo T J, Seol D J and Oh K H 2000 *Metall. Mater. Trans. B.* **31** 779
[19] Won Y M, Kim K, Yeo T and Oh K H 1998 *ISIJ Int.* **38** 1093
[20] Schmidtmann E and Rakoski F 1983 *Arch. Eisenhüttenwes* **54** 357
[21] Shin G, Kajitani T, Suzuki T and Umeda T 1992 *Tetsu- to- Hagane* **78** 587
[22] Seol D J, Won Y M, Oh K H, Shin Y C and Yim C H 2000 *ISIJ Int.* **40** 356
[23] Nakata H and Yasunaka H 1990 *Tetsu-to-Hagane* **76** 376
[24] Nakagawa T, Umeda T, Murata J, Kamimura Y and Niwa N 1995 *ISIJ Int.* **35** 723
[25] Suzuki G H, Nishimura S and Nakamura Y 1984 *Trans. Iron Steel Ins. Jpn.* **24** 54
[26] Yu C H, Suzuki M, Shibata H and Emi T 1996 *Mater. Trans. Japan Inst. Metals.* **37** 1251
[27] Weinberg F 1979 *Metall. Trans.* **10B** 219
[28] Bale C W, Chartrand P, Eriksson G, Jung I H, Kang Y B and Pelton A D 2009 *CALPHAD* **33** 295